DIGITALCOMMONS
@WAYNESTATE

Wayne State University

Wayne State University Theses

1-1-2016

A Five Residue Insertion Between Codons 28 And 29 Of The Hiv-1 Protease Gene Reduces The Replicative Capacity Of The Virus

Cathy Mcleod
Wayne State University,

Follow this and additional works at: https://digitalcommons.wayne.edu/oa_theses

 Part of the Biochemistry Commons

Recommended Citation
Mcleod, Cathy, "A Five Residue Insertion Between Codons 28 And 29 Of The Hiv-1 Protease Gene Reduces The Replicative Capacity Of The Virus" (2016). *Wayne State University Theses*. 496.
https://digitalcommons.wayne.edu/oa_theses/496

This Open Access Thesis is brought to you for free and open access by DigitalCommons@WayneState. It has been accepted for inclusion in Wayne State University Theses by an authorized administrator of DigitalCommons@WayneState.

A FIVE RESIDUE INSERTION BETWEEN CODONS 28 AND 29 OF THE HIV-1 PROTEASE GENE REDUCES THE REPLICATIVE CAPACITY OF THE VIRUS

by

CATHY MCLEOD

THESIS

Submitted to the Graduate School

of Wayne State University,

Detroit, Michigan

in partial fulfillment of the requirements

for the degree of

MASTER OF SCIENCE

2016

MAJOR: BIOCHEMISTRY AND
MOLECULAR BIOLOGY

Approved by:

_____

Advisor Date

TABLE OF CONTENTS

LIST OF TABLES

LIST OF FIGURES

Chapter 1: Introduction

1.1 HIV-1 Viral Infection

According to estimates by the CDC, as of 2011 there were more than 1.2 million people living with HIV in the United States. The risk of HIV infection continues to be a serious public health concern; over the past two decades, incidence of HIV infection has stabilized at approximately 50,000 new infections per year in the US. Of those infected, men who have sex with men (MSM), African Americans and those of Latin American descent, are disproportionately affected. In the rest of the world, HIV infection also remains an issue, with about 2.1 million new cases of HIV being reported in 2013. There are an estimated 35 million people living with HIV around the world, with sub-Saharan Africa most heavily affected by the disease [CDC.gov/HIV/statistics/overview].

1.2 HIV-1 Protease

HIV-1 protease (PR) is a 99 amino acid homo-dimeric enzyme. The two monomers of the PR form a central active site channel which contains the catalytic residues Asp 25 and Asp 25'. HIV PR is responsible for the maturation of virions by cleaving the Gag and GagPol polyprotein precursors into functionally active proteins [1][2]. The Gag precursor is cleaved into the structural proteins including the matrix, capsid, nucleocapsid, and spacer peptides p1, and p2. The Pol precursor is cleaved into the viral enzymes protease, reverse transcriptase and integrase [1]. As HIV-1 PR plays such an essential role in the HIV-1 viral life cycle, it has become an attractive and successful target for drug development.

1.3 HIV-1 PR Inhibitors

To combat HIV infection, highly active anti-retroviral therapy (HAART) remains the standard of care, with protease inhibitors (PIs) playing an essential role. HAART typically consists of a cocktail of anti-retroviral drugs including two nucleoside reverse transcriptase inhibitors (NRTIs), along with either a non-nucleoside reverse transcriptase inhibitory (NNRTI) or a PI. HAART combinations including PIs have been typically more effective than combinations that do not include PIs, and monotherapies [3].

There are currently nine PIs approved for use by the FDA: Ritonavir (RTV), Lopinavir (LPV), Atazanavir (ATV), Darunavir (DRV), Saquinavir (SQV), Indinavir (IDV), Nelfinavir (NFV), Tipranavir (TPV) and Fosamprenavir (FPV). PIs inhibit PR by binding to the active site residues, competing with the natural substrate peptides. PIs have been designed to mimic the natural transition state of the peptide, where the PI hydroxyl interacts with the carbonyl of Asp 25 and Asp 25' in the HIV PR active site, thus inactivating the enzyme [4]. Unfortunately, drug resistance PR mutations have been associated with each PI. Because of their similar structure, and mechanism of action, it is common for cross resistance to occur between PIs , resulting in treatment failure [4][5]. Mutations in regions flanking the binding pocket of HIV-1 protease are typically seen in PI resistance, because in this area the mutations will interfere with inhibitor binding but not Gag and GagPol binding [6].

1.4 HIV-1 PR and Drug Resistance

Though PIs have been effective at reducing HIV related deaths, resistance to these drugs occurs when mutations in the PR lead to reduced binding affinity of the PR for the inhibitor, while interactions between the PR and substrate remain [7]. Thus, inhibitors are unable to bind and block enzyme activity, while substrate continues to bind and be cleaved by the PR.

Mutations which lead to PI resistance occur in large part due to the highly error prone reverse transcriptase and its lack of proof reading ability. As PR mutations accumulate in the viral population, there is an increase in genetic diversity; an evolutionary advantage for the virus which under drug induced selective pressure allows for PR with these mutations to proliferate if they confer a survival advantage in the presence of a PI. Non-compliance with HAART therapy can accelerate the process of selecting drug resistant mutants [5].

These mutations affect drug-PR interactions in a variety of ways, depending on the type of mutation present. Amino acid substitutions in the PR active site, called primary mutations, account for the majority of PI resistance and directly alter drug-PR interactions, resulting in the inability of the drug to bind and efficiently block enzyme function [5][7]. Primary mutations may result in cross-resistance due to PIs being similar in structure, but they may also reduce the catalytic activity of the PR as well [7]. Resistance mutations may also occur at the dimer interface disrupting the interactions between the two monomers. Changes in the interaction network between the two monomers of PR, could result in dissociation of the dimer and release the PI from the active site [5]. Mutations distant from the active site have also been shown to confer resistance by altering interactions indirectly between necessary water molecules, and enzyme dynamics. These distant mutations may also in some ways modulate the activity of major resistance mutations in ways that are not immediately apparent [5]. Mutations in the PR are not always substitutions, insertions have been documented in the literature, though their mechanism of action and the role they play in PI resistance remains unclear.

1.5 HIV-1 PR Insertion Mutations

Of all mutations, insertions in the HIV protease remain among the most understudied in the literature. Protease insertions typically occur as repeating sequences of neighboring amino acids, and the proposed mechanism by which insertions are formed is thought to be due to slipping of the reverse transcriptase [8][9]. Insertions occur at many different positions in the HIV protease, but tend to occur near external loops and turns, especially in larger insertions of more than five amino acids. Insertions in the PR are thought to be rare, in one study comprising only 0.1% of mutations in a sample population between 1999-2000 [8]. Insertions themselves are not shown to have an effect on resistance to PIs. A 2001 study showed that no real difference existed in drug susceptibility between multi-drug resistant (MDR) isolates containing an insertion, and non-insertion containing isolates [10]. This suggests that the PI resistance mutations (rather than the insertion) were responsible for decreased susceptibility to PIs [10]. However, some evidence suggests that insertions may in fact be compensatory to resistance mutations . These data suggest that MDR proteases containing an insertion show a boost in substrate cleavage, and replicative capacity [8].

1.6 HIV-1 PR Clinical Isolate

At present, there are no modeling studies of an insert-containing PR isolate. We report a detailed modelling study of an isolate containing a 5-residue insertion between codons 28 and 29 (MDR/28). This isolate was obtained from a patient at the Wayne State University Infectious Disease Clinic in Detroit, MI. The patient is poorly adherent with antiretroviral therapy. MDR/28 is the first isolate at this facility to contain an insertion of this size. Additionally, this isolate displays *reduced* replicative capacity compared to the WT virus, as it is expected most mutations will reduce replicative capacity. To structurally characterize the impact of the MDR/28 insertion,

a homology model was created and compared to a wild-type crystal structure and a protease model containing the MDR mutations with the insert removed. Each protease model was then docked with protease inhibitors (PI) and cleavage peptide CA/p2 [11]. Molecular dynamics simulations were performed for each of the complexes using NAMD [12].

Chapter 2: Materials and Methods

2.1 Phenotypic and Genotypic Reports

Phenotypic reports regarding the mutant MDR/28 PR were obtained from a Phenosense® HIV drug resistance test, ordered by the Detroit Medical Center [13]. Phenosense provides a quantitative measurement of how well the clinical isolate responds to antivirals, including nucleoside reverse transcriptase inhibitors (NRTIs), nonnucleoside reverse transcriptase inhibitors (NNRTIs) and protease inhibitors (PIs). This report also includes replicative capacity data.

Viroseq® HIV-1 genotyping system was used at the Detroit Medical Center in order to obtain genotypic data on the clinical isolate PR [14]. This system screens against software to identify known resistance mutations.

2.2 Homology Modeling

A homology model of MDR/28 PR was created using Schrödinger Prime [15]. 2O4S.pdb was obtained from the Protein Data Bank (rcsb.org) and was used to build the model. 2O4S exhibits 82% sequence identity to the insertion isolate MDR/28, and was chosen as it provides the highest sequence homology available for all PR structures in dimer form [16]. A model was created of MDR PR, with the insertion removed, also using 2O4S.pdb as a template.

2.3 Molecular Dynamics Simulation

2.3.1 Protease Complex Preparation

Sixteen systems underwent molecular dynamics simulations, including apo structures of WT HIV-1 PR, MDR/28 PR, and MDR PR, as well as all PR models with ligands bound. The ligands used for the simulations were DRV, ATV, LPV, SQV, and CA/p2. To obtain proper coordinates for the ligands, the homology models and WT PR were aligned to pdb entries 4DQV (DRV) [17], 2NNP (SQV) [18], 3EKY (ATV) [19], 4L1A (LPV) [20], and 3OUD (CA/p2) [21], using Pymol to obtain proper coordinates [22].

2.3.2 System Preparation

The preparation of the system for MD simulation was carried out using Visual Molecular Dynamics software (VMD v.1.9.2) [11]. The PR complexes as well as apo structures were placed in a 12 Å TIP3P water box and were then neutralized with 0.15 M $MgCl_2$. Simulations were performed for 40 ns using NAMD (e) V 2.9 [23] and CHARMM force field 36 [24] to set parameters. The Particle Mesh Ewald (PME) method was used to calculate long range coulomb interactions. Temperature was maintained at 300 K using Langevin dynamics and pressure maintained at 1 atm using the Nose-Hoover Langevin piston method. All simulations were run using one of two different computing clusters, the Wayne State University Grid (www.grid.wayne.edu) or Stampede at the Texas Advanced Computing Center (http://www.tacc.utexas.edu).

2.4. Structural Analysis

Distance measurements and secondary structural analysis were carried out using VMD [11]. Analysis of the PR active site volume was carried out using Caver analyst, to visualize and measure the active site channel over the 40ns trajectory [25]. The volume of each tunnel was

averaged for the whole simulation. To study the interactions between the PR and peptide, Ligplot+ was used to visualize hydrogen bonds and VdW interactions [26]. These too were averaged for each PR complex over the length of the MD trajectory.

2.5 Docking and Affinity Estimation

In order to quantify a difference in binding affinity between the WT PR and mutant MDR/28, MM-GBSA calculations were performed using the Prime function of Schrodinger software [27]. MM-GBSA method calculates the free energy of binding through the use of molecular mechanics and implicit solvation models, where the binding energy=ΔE(complex)- ΔE (ligand)-ΔE(substrate). [27]. In preparation for MM-GBSA analysis, the WT, MDR/28 and MDR PR and ligands were prepared using the protein preparation wizard and ligprep functions (Schrodinger release 2014) [28], respectively. Subsequently, induced fit docking with Glide was performed to accommodate various ligands in each PR active site [29]. The resulting Glide poses were used as input for the MM-GBSA affinity estimation, and their energy scores were averaged for each ligand.

Chapter 3: Results

3.1 MDR/28 HIV PR mutant exhibits resistance to multiple protease inhibitors and displays reduced replicative capacity

Phenosense® susceptibility testing of MDR/28 revealed full or partial resistance to the following PIs: atazanavir (ATV/r), amprenavir (AMP/r), indinavir (IDV/r), tipranavir (TPV), and nelfinavir (NFV) **(Table 1)**. It was also determined in a Phenosense® replicative capacity assay that in the absence of inhibitors the isolate MDR/28 functioned at a reduced replicative capacity compared to WT **(Fig 2).**

Genotyping with Viroseq® showed MDR/28 contained resistance mutations impacting the affinity of the PIs IDV, LPV, fosamprenavir (FPV), as well as conferring possible resistance to TPV, DRV, and ATV. Saquinavir (SQV) was the only inhibitor for which there were no known resistance mutations present **(Table 1)**. A list of resistance mutations found in MDR/28 and their contributions are listed in **Fig 1.b.**

	ATV/r	DRV/r	FPV/r	IND/r	LPV	NFV	RTV	SQV/r	TPV/r
Phenotype	Resistant	Partially Susceptible	Resistant	Resistant	Partially Susceptible	Resistant	Resistant	Susceptible	Partially Susceptible
Genotype	Possible Resistance	Possible Resistance	Resistant	Resistant	Resistant	Resistant	N/A	Susceptible	Partially Susceptible

Table 1: **Phenotypic and genotypic susceptibility data.** The phenotypic and genotypic resistance data provided by Phenosense® and Viroseq® reports are summarized in the table above. For detailed genotypic information see the resistance mutation key for MDR/28 in **Fig 1.**

3.1.1 Discussion

Phenotype and genotype testing revealed that the clinical HIV-1 PR isolate was multi-drug resistant (MDR) and contained a five residue insertion at position 28 of the HIV-1 PR gene. Comparison between phenotypic and genotypic data showed that though the two assays agreed relatively well, there were some drugs for which the phenotypic and genotypic resistance data differed **(Table 1)**. For our purposes, we used the phenotypic results in order to choose drugs to complex with our PR models. Genotypic reports tend to be more predictive of future drug resistance, as they detect mutations which may only cause resistance if accompanied by other mutations that modulate their activity. We are interested in the clinical outcome [i.e. the phenotypic data]. We determined that DRV, ATV, and LPV were the PIs most

clinically relevant at the current time and as such were chosen for simulation. SQV was used as well as it is the only PI that MDR/28 was shown to be susceptible to in both assays.

1.a.

(1)PQITLWQRPVVTIKVGGKLKEALLDTGADDTILDDTILEEMDLPGRWKPKIIGGIGGFLRVRQYDQIPIEICG HKVIGTVVVGPTPMNIIGRNLLTQLGCTLNF(104)

1.b.

Mutation	Requires additional mutation	Possible resistance	Resistance	Resistance countered
L10V	TPV,IDV,SQV,DRV,ATV,NFV,FPV	LPV		
V32I	TPV,IDV,LPV,DRV,ATV,NFV,FPV			
M46I	TPV, IDV,LPV,ATV,FPV	NFV		
I54L	IDV,SQV,LPV,DRV,ATV	NFV	FPV	
A71V	TPV,IDV,SQV,LPV,ATV			
L76V	DRV	IDV,LPV	FPV	TPV
V82M	TPV,IDV,LPV,ATV,NFV,FPV			

Fig 1. Sequence of the MDR/28 isolate and resistance mutations. (a): The amino acid sequence for MDR/28 PR is shown above, with the insertion residues colored in purple. The MDR mutations are colored in red. **(b)**: The genotype of MDR/28 clinical isolate is summarized below according to the Viroseq® HIV-1 genotyping system report.

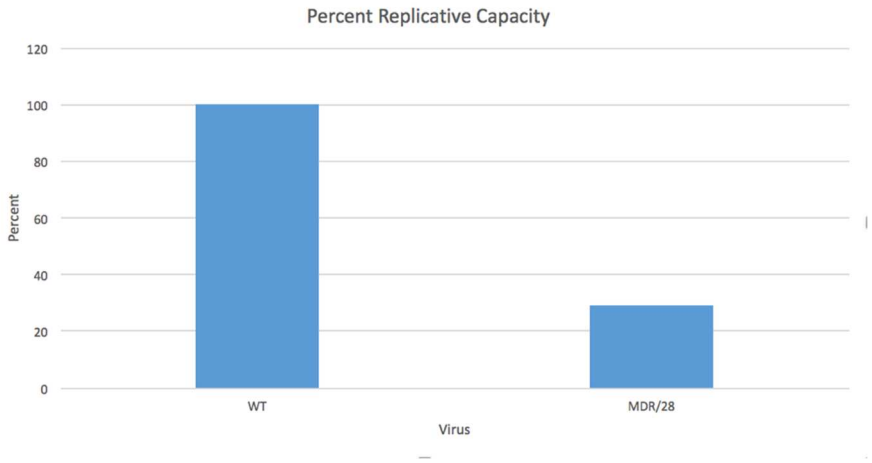

Fig 2. Viral replicative capacity of MDR/28. The replicative capacity of MDR/28 mutant virus is shown as compared to a WT virus. MDR/28 displayed an average replicative capacity of only 29% of WT.

3.2 The active site volume of MDR/28 is increased compared to wild type

The active site channel of MDR/28 initially appeared to be smaller in volume than WT PR **(Fig 3.a)**. To confirm this observation, Caver analyst was used to compute the length and bottleneck radius of the active site channel of each PR over the course of the simulation, showing that in fact MDR/28 active site volume increases as the simulation progresses [25]**(Fig 3.b).** From this, we calculated the average total volume of each channel, MDR/28 was shown to have a greater active site channel volume than WT PR by about 16%, contrary to our initial observation **(Fig 3.c).**

The solvent accessible surface area (SASA) of the catalytic residues Asp 25 and Asp 25' was measured using the VMD timeline plugin [11]. The SASA of MDR/28 was observed to be slightly higher than that of WT by 3 $Å^2$ **(Fig 4)**.

3.2.1 Discussion

Previous studies have shown that an increase in the PR active site volume results in a weaker binding to substrate, due to the loss of important interactions between the PR and

substrate [30]. It follows that the increased active site volume of MDR/28 PR when compared to WT, observed in our analysis, will result in a loss of interactions between active site residue side chains and substrate.

It is worth noting that the increased active site channel volume was seen as a result of the MD simulation, wherein one of the flap tips of MDR/28 was observed to curl back on itself. It is possible that this curling back of the flap may result in the spike seen in active site volume from the 29th to 32nd ns **(Fig 3.b).** For this reason, we calculated the SASA, and although there is only a 3 Å^2 increase in the binding site (surface area) of MDR/28, this may be sufficient to disturb interactions between PR and substrate **(Fig 3.c).** MDR PR that exhibit only a 3.0 Å^2 increased active site volume have been associated with high level resistance over WT PR [31]. For this reason, we assert that because MDR/28 displays a predicted expansion of SASA area and active site volume, these may lead to a loss of important interactions with substrate.

3.a

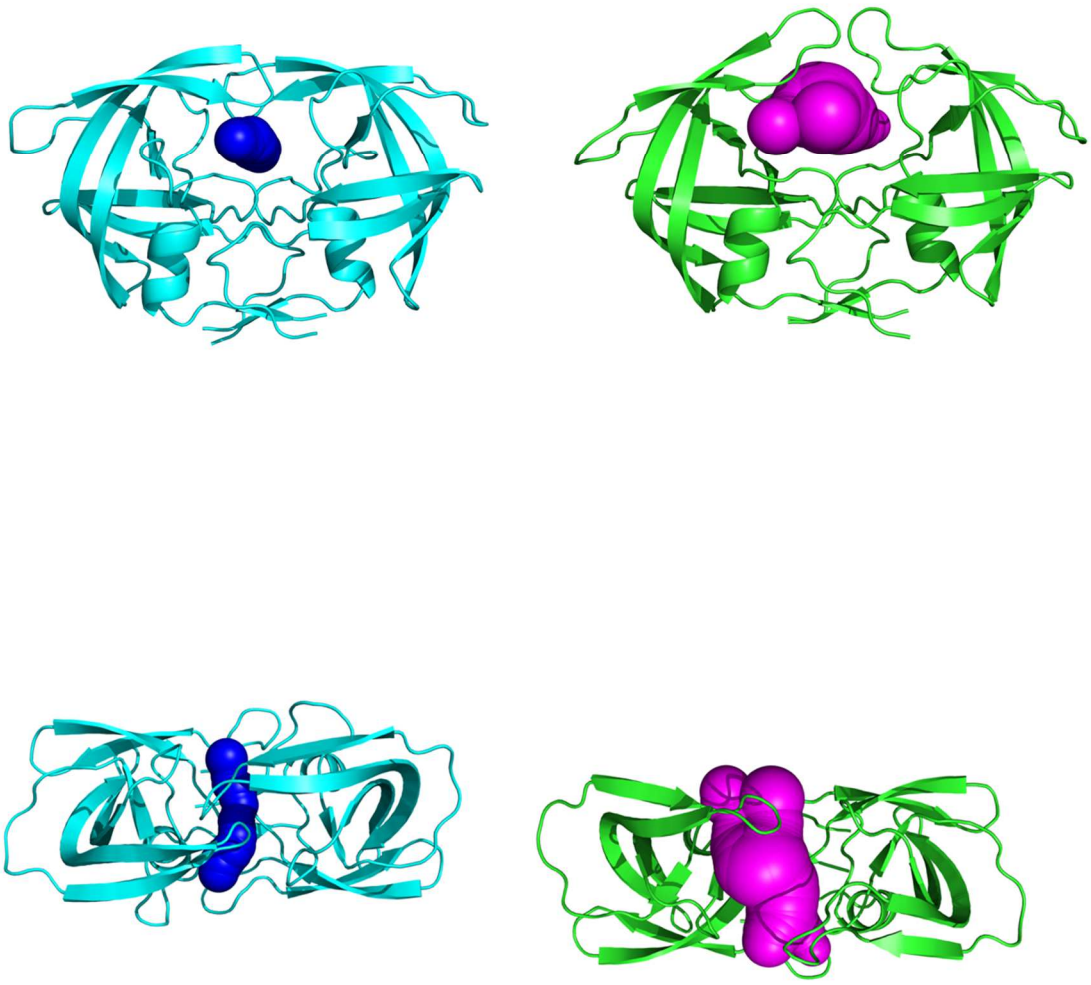

3.b

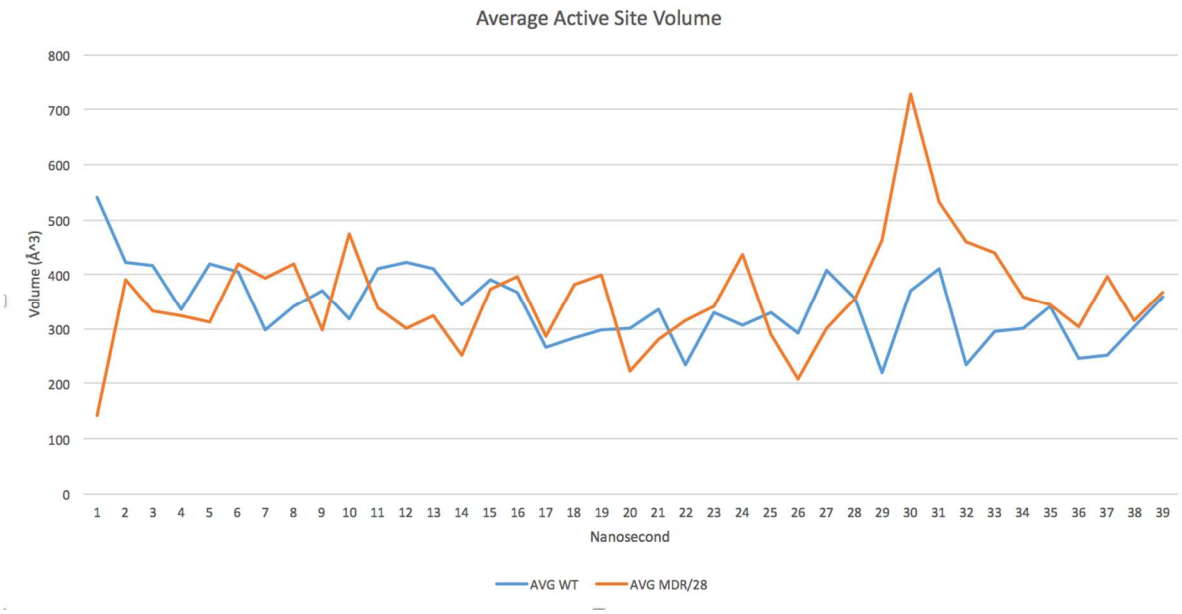

3.c

Protease	Total Average Volume (Å^3)
WT	340
MDR/28	359

Fig 3. The active site volume of MDR/28 relative to WT. (a): From left MDR/28 PR is shown in cyan, with its corresponding channel volume colored in blue. On the right WT PR is shown in green with its channel volume in magenta. The channels were calculated using the caver plugin for Pymol, and represent the active site volume post energy minimization. **(b)**: The average active site volume over the course of the 40ns simulation is shown. **(c)**: The total average volume for the active site channels is presented, this represents the average for all channels over 40ns.

4.a

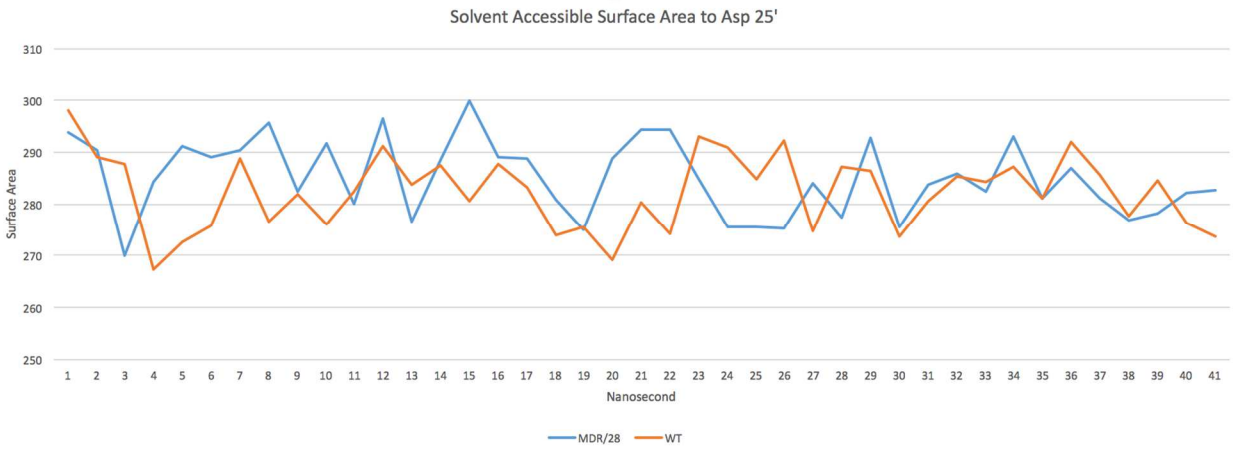

4.b

PR	AVG SASA
MDR/28	285
WT	282

Fig 4. Solvent available surface area for catalytic residues. (a) The solvent accessible surface area is shown over the course of a 40ns simulation for residues Asp 25 and Asp 25' of MDR and WT PR. **(b)** The average SASA for each PR is compared. Values were determined to be statistically significant by one-way ANOVA $p < 0.05$.

3.3 Peptide binding to MDR/28 is shifted to one side of the active site

In a superimposed view of MDR/28 and WT PR in complex with the CA/p2 peptide, the peptide appeared to be displaced in the MDR/28 active site after energy minimization was completed **(Fig 5)**. To quantify this displacement, the distance between the PRs was measured at the scissile bond carbon using VMD [11]. MDR/28 had shifted 2.9 Å to one side of the active site compared to the WT complex.

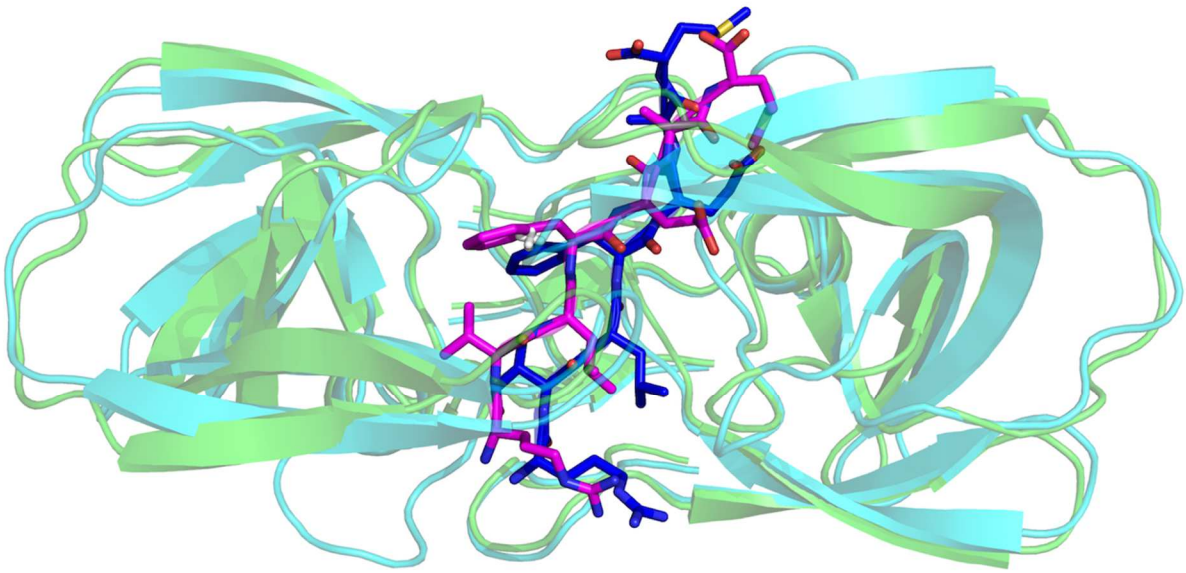

Fig 5. **Superimposed view of MDR/28 and WT peptides.** Above view of superimposed MDR/28 PR (cyan) and WT (green) PR in complex with peptide CA/p2. The peptide MDR/28 shown in blue is displaced towards one side of the active site when compared to the WT peptide in magenta. This figure is a representation of frame 21 of the trajectory.

In order to confirm that this displacement of the peptide was consistent over the entire 40ns MD trajectory, measurements were taken for each of the PR complexes, measuring the distance from each Asp 25 gamma carbon (for ease of measurement) to the scissile carbonyl carbon of the peptide over the course of the entire simulation **(Fig 6).** This analysis revealed that as the simulation progressed, the peptide in the MDR/28 complex moved further away from Asp 25. The initial distance was 5.23 A at the beginning of the simulation and increased to 8.74 Å by the end, averaging 8.60 Å for the whole simulation. In contrast, in the WT complex the CA/p2 peptide was seen to move from 4.71 Å to 5.54 Å away from Asp 25, averaging only 5.36 Å.

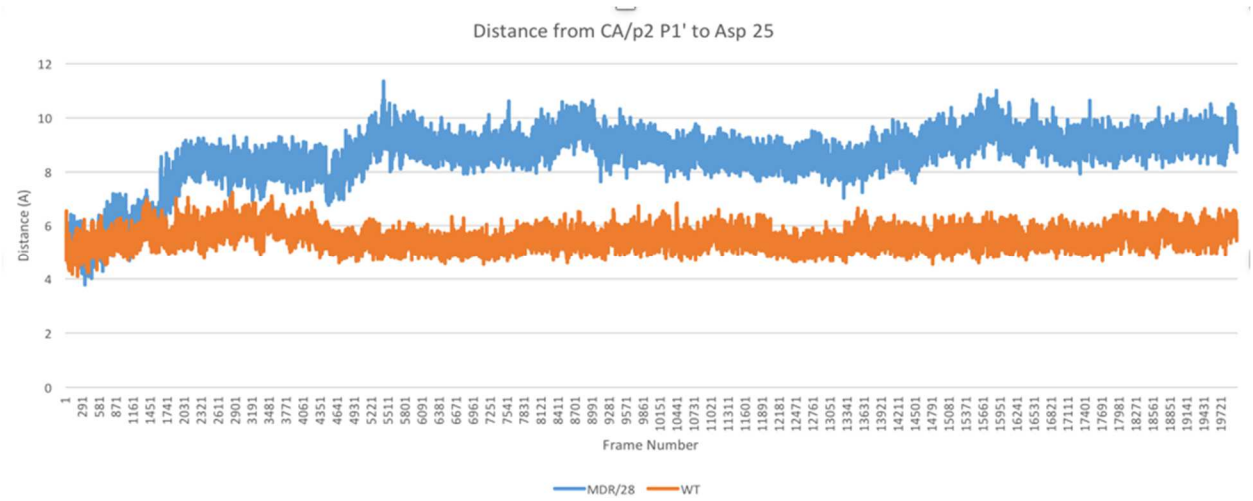

Fig 6. Distance measurements between the peptide and catalytic residue. The distance from the CA/p2 scissile carbonyl to the gamma-carbon of Aspartate 25 over the course of 20,000 frames is shown. MDR/28 in blue, WT in orange. The peptide appears to be moving increasingly further from the catalytic residue.

3.3.1 Discussion

The migration of the peptide away from catalytic residues that is observed in the MDR/28 complex is a result of missing interactions (to be determined in later analysis) which are needed to allow peptide to bind in the active site for catalysis. It is known that the recognition and binding of peptide in the PR active site is largely dependent on the shape and size of the peptide in question [32]. An increased PR active site may not correctly recognize the peptide thus allowing it to move out of the active site without being cleaved. There is another structural feature that may account for a lack of interactions between PR-and peptide: secondary structure.

3.4 The MDR/28 insertion causes local secondary structural changes

In order to see if any secondary structural changes were induced by the insertion that could account for lost interactions, Ramachandran analysis was performed for residues 25 through 35. Residues were chosen that flank the insertion on both sides, omitting the insertion residues themselves. This analysis revealed that compared to WT PR, MDR/28 shows a marked change in secondary structure at residues 29 and 30 **(Fig 7).** At residue 29 a right-handed alpha helix conformation normally present in WT is changed to a beta sheet conformation in MDR/28. Residue 30 displays the opposite effect, with the normal beta sheet conformation being transiently changed to alpha helical over the course of the simulation. No other residues which surrounded the insertion showed a change in secondary structure.

MDR PR, which functioned as a control, showed no change in secondary structure when compared to WT. This is evidence that the five residue insertion at residue 28 transiently affects the secondary structure of neighboring residues.

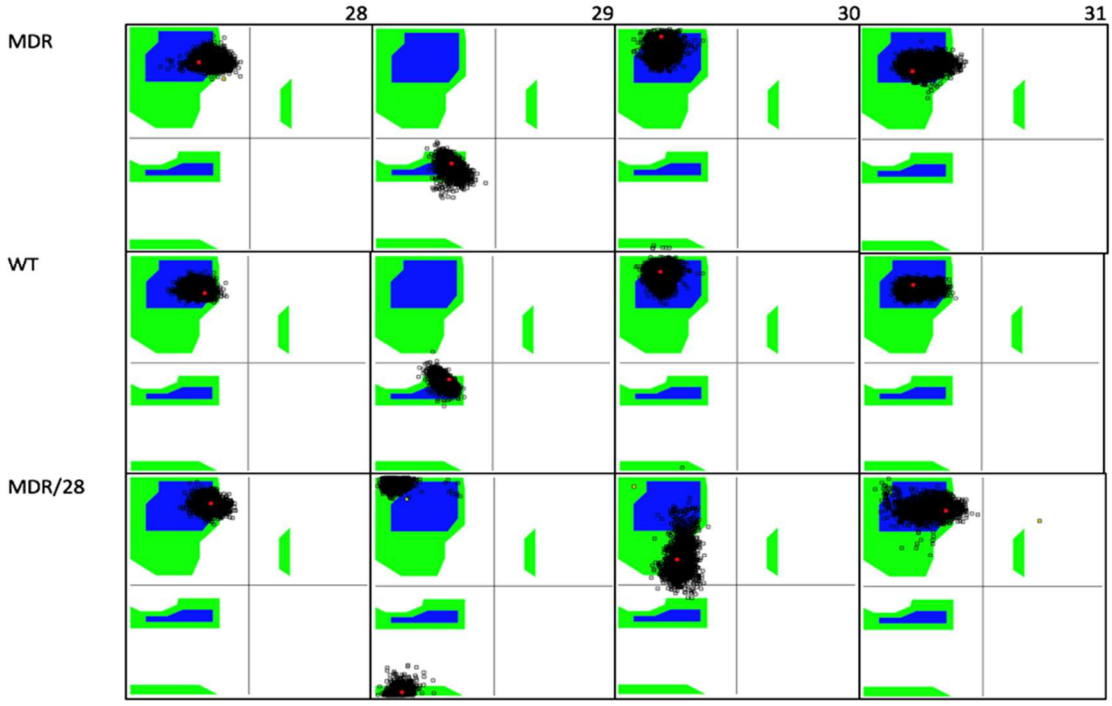

Fig 7.: **Secondary structural analysis of insert flanking residues**. Ramachandran plot analysis of secondary structure for each PR, residues 28-31 are pictured above. The residues were chosen to analyze changes in PR structure on either side of the insertion sequence, and the insertion itself was not included. Notice the change in secondary structure from WT to MDR/28 at residues 29 and 30 in particular.

3.4.1 Discussion

In addition to increased active site volume, the changes in secondary structure at residues 29 and 30 may contribute to the loss of interactions in MDR/28 compared to WT PR. Prior research illustrates that peptide interactions with PR residues 29 and 30 are responsible for the specificity of the PR for CA/p2 peptide cleavage site [31]. These residues are also known to make hydrogen bonds to the backbone of all cleavage peptides and residue 30 is known to contribute to specificity

by making side chain hydrogen bonds to either Glu or Gln residues present in peptides CA/p2, p2/NC, and p1/p6 [30]. The changing of secondary structure of these residues could have implications in reducing the number of interactions between PR and peptide.

3.5 Hydrogen bonds and VdW interactions are lost in MDR/28 compared to WT

To investigate if the previous structural changes (increased active site and secondary structural changes) contribute to a loss of interactions between the PR and peptide, Ligplot+ analysis was used. Every 4ns throughout the MD simulation, the hydrogen bonds and VdW interactions were calculated for each PR complex, and the total interactions present at each frame measured across the whole simulation were averaged. Any interactions which were lost in MDR/28 compared to WT were noted (**Table 2**). MDR/28 PR lost a total of four hydrogen bonds to the peptide, and five VdW interactions which were present in the WT complex.

Hydrogen bonds lost	VdW interactions lost
Asp 30	Val 82
Gly 48	Val 32
Gly 49	Met 46
Ala 28	Arg 8
	Asp 29

Table 2. Interactions lost between MDR/28 PR and peptide. The lost interactions of MDR/28 with peptide are shown when compared to WT. Both hydrogen bonds and VdW interactions were investigated over 40ns.

3.5.1 Discussion

Of interest among the lost interactions are VdW interactions to residue 29 and hydrogen bonding to residue 30. As previously stated these two residues are important in peptide recognition and specificity. The fact that these residues are altered in MDR/28, and interactions are lost to them is further evidence that the insertion has induced a change in the PR which results in its inability to bind tightly to substrate. Gly 48 is likewise considered a conserved bond among all PR and Gagpol interactions, and is also missing in MDR/28. The loss of such important interactions implies that binding affinity between PR and substrate may be negatively affected in MDR/28, and thus lead to a reduced replicative capacity.

3.6 MM-GBSA binding affinity data shows MDR/28 has decreased affinity for substrate and ligands

A loss of interactions between the PR and peptide suggests decreased binding affinity. Data from MM-GBSA calculations showed that ligands were predicted to bind more tightly to WT PR than MDR/28 PR **(Fig 8).** The difference in binding affinity that was observed between MDR/28, MDR and WT PR was determined to be statistically significant by single factor ANOVA for all ligands. All PIs and CA/p2 in complex with MDR/28- displayed a decreased binding energy of at least 26% (for SQV) and up to 36% (for LPV) (compared to WT).

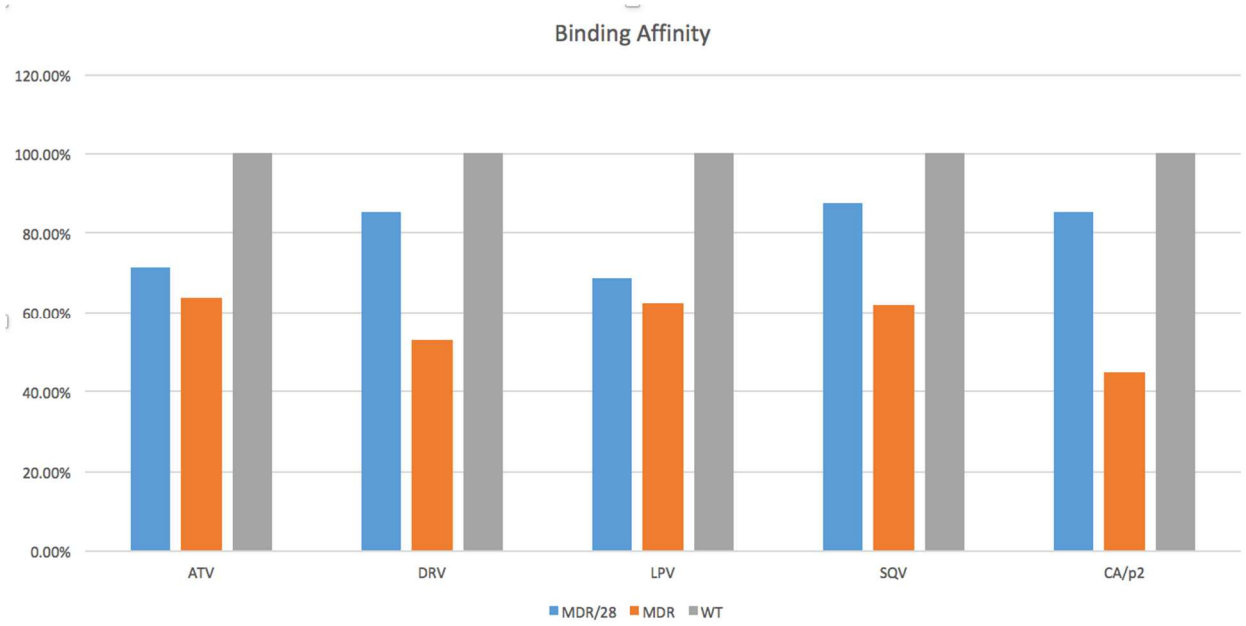

Fig 8.: **Binding affinity data for PR complexes.** The normalized binding energy of PR complexes was determined using the MM-GBSA function of Schrodinger Prime software. The binding energy data is a normalized average for each complex, as each drug had numerous possible poses in the PR active site. For each ligand $p < 0.05$.

3.6.1 Discussion

MM-GBSA analysis predicted MDR/28 has a worse affinity for substrate than WT, as our previous data had suggested. Interestingly MDR/28 has a better binding affinity than the MDR control, suggesting that there is a compensatory effect to the insertion. The decrease in binding affinity of MDR/28 as a result of lost interactions, may result in the displaced peptide and its subsequent migration from the catalytic residues seen during the 40ns MD simulation.

Conclusions

Our goal was to elucidate the mechanism of reduced replicative capacity in a mutant-bearing PR with an insertion at residue 28. Structural changes in the PR introduced by the insertion (such as the increased active site volume and secondary structural changes of residues 29 and 30), resulted in a loss of hydrogen bonds and VdW interactions between the PR active site and the peptide CA/p2. The loss of necessary contacts leads to decreased affinity of MDR/28 for peptide, which allows for the displacement of the peptide in the active site and its migration away from the catalytic residues. Without proper interactions between the PR and peptide, the peptide is unable to be held in the proper conformation for cleavage, and mature proteins will not result. This could result in a reduced replicative capacity for the virus. No mechanism of the effect of the insertion (rather than other MDR mutations) on PIs was seen in the data.

REFERENCES

[1] A. Fun, A.M.J. Wensing, J. Verheyen, M. Nijhuis, Human Immunodeficiency Virus Gag and protease: partners in resistance., Retrovirology. 9 (2012) 63. doi:10.1186/1742-4690-9-63.

[2] P.D. Yin, D. Das, H. Mitsuya, Overcoming HIV drug resistance through rational drug design based on molecular, biochemical, and structural profiles of HIV resistance., Cell. Mol. Life Sci. 63 (2006) 1706–1724. doi:10.1007/s00018-006-6009-7.

[3] F.J.J. Palella, K.M. Delaney, A.C. Moorman, M.O. Loveless, J. Fuhrer, G.A. Satten, et al., Declining morbidity and mortality among patients with advanced human immunodeficiency virus infection. HIV Outpatient Study Investigators., N. Engl. J. Med. 338 (1998) 853–860. doi:10.1056/NEJM199803263381301.

[4] Z. Lv, Y. Chu, Y. Wang, HIV protease inhibitors: a review of molecular selectivity and toxicity., HIV. AIDS. (Auckl). 7 (2015) 95–104. doi:10.2147/HIV.S79956.

[5] I.T. Weber, J. Agniswamy, HIV-1 Protease: Structural Perspectives on Drug Resistance, Viruses. 1 (2009) 1110–1136. doi:10.3390/v1031110.

[6] M.N.L. Nalam, A. Ali, M.D. Altman, G.S.K.K. Reddy, S. Chellappan, V. Kairys, et al., Evaluating the substrate-envelope hypothesis: structural analysis of novel HIV-1 protease inhibitors designed to be robust against drug resistance., J. Virol. 84 (2010) 5368–5378. doi:10.1128/JVI.02531-09.

[7] P. Iyidogan, K.S. Anderson, Current perspectives on HIV-1 antiretroviral drug resistance., Viruses. 6 (2014) 4095–4139. doi:10.3390/v6104095.

[8] M.A. Winters, T.C. Merigan, Insertions in the Human Immunodeficiency Virus Type 1

Protease and Reverse Transcriptase Genes: Clinical Impact and Molecular Mechanisms, Antimicrob. Agents Chemother. 49 (2005) 2575–2582. doi:10.1128/AAC.49.7.2575-2582.2005.

[9] G.P. Harrison, M.S. Mayo, E. Hunter, A.M. Lever, Pausing of reverse transcriptase on retroviral RNA templates is influenced by secondary structures both 5’ and 3' of the catalytic site., Nucleic Acids Res. 26 (1998) 3433–42. http://www.pubmedcentral.nih.gov/articlerender.fcgi?artid=147721&tool=pmcentrez&rendertype=abstract (accessed May 20, 2015).

[10] E.-Y. Kim, M.A. Winters, R.M. Kagan, T.C. Merigan, Functional Correlates of Insertion Mutations in the Protease Gene of Human Immunodeficiency Virus Type 1 Isolates from Patients, J. Virol. 75 (2001) 11227–11233. doi:10.1128/JVI.75.22.11227-11233.2001.

[11] W. Humphrey, A. Dalke, K. Schulten, VMD: visual molecular dynamics., J. Mol. Graph. 14 (1996) 27–28,33–38.

[12] J.C. Phillips, R. Braun, W. Wang, J. Gumbart, E. Tajkhorshid, E. Villa, et al., Scalable molecular dynamics with NAMD., J. Comput. Chem. 26 (2005) 1781–802. doi:10.1002/jcc.20289.

[13] C.J. Petropoulos, N.T. Parkin, K.L. Limoli, Y.S. Lie, T. Wrin, W. Huang, et al., A novel phenotypic drug susceptibility assay for human immunodeficiency virus type 1., Antimicrob. Agents Chemother. 44 (2000) 920–928.

[14] S. Cunningham, B. Ank, D. Lewis, W. Lu, M. Wantman, J.A. Dileanis, et al., Performance of the applied biosystems ViroSeq human immunodeficiency virus type 1 (HIV-1) genotyping system for sequence-based analysis of HIV-1 in pediatric plasma samples., J. Clin. Microbiol. 39 (2001) 1254–1257. doi:10.1128/JCM.39.4.1254-

1257.2001.

[15] M.P. Jacobson, D.L. Pincus, C.S. Rapp, T.J.F. Day, B. Honig, D.E. Shaw, et al., A hierarchical approach to all-atom protein loop prediction., Proteins. 55 (2004) 351–367. doi:10.1002/prot.10613.

[16] S. Muzammil, A.A. Armstrong, L.W. Kang, A. Jakalian, P.R. Bonneau, V. Schmelmer, et al., Unique thermodynamic response of tipranavir to human immunodeficiency virus type 1 protease drug resistance mutations., J. Virol. 81 (2007) 5144–5154. doi:10.1128/JVI.02706-06.

[17] S. Mittal, Y. Cai, M.N.L. Nalam, D.N.A. Bolon, C.A. Schiffer, Hydrophobic core flexibility modulates enzyme activity in HIV-1 protease., J. Am. Chem. Soc. 134 (2012) 4163–4168. doi:10.1021/ja2095766.

[18] Y. Tie, A.Y. Kovalevsky, P. Boross, Y.-F. Wang, A.K. Ghosh, J. Tozser, et al., Atomic resolution crystal structures of HIV-1 protease and mutants V82A and I84V with saquinavir., Proteins. 67 (2007) 232–242. doi:10.1002/prot.21304.

[19] N.M. King, M. Prabu-Jeyabalan, R.M. Bandaranayake, M.N.L. Nalam, E.A. Nalivaika, A. Ozen, et al., Extreme entropy-enthalpy compensation in a drug-resistant variant of HIV-1 protease., ACS Chem. Biol. 7 (2012) 1536–1546. doi:10.1021/cb300191k.

[20] Z. Liu, R.S. Yedidi, Y. Wang, T.G. Dewdney, S.J. Reiter, J.S. Brunzelle, et al., Crystallographic study of multi-drug resistant HIV-1 protease lopinavir complex: mechanism of drug recognition and resistance., Biochem. Biophys. Res. Commun. 437 (2013) 199–204. doi:10.1016/j.bbrc.2013.06.027.

[21] Z. Liu, Y. Wang, J. Brunzelle, I.A. Kovari, L.C. Kovari, Nine crystal structures determine the substrate envelope of the MDR HIV-1 protease., Protein J. 30 (2011) 173–183.

doi:10.1007/s10930-011-9316-2.

[22] W.L. DeLano, The PyMOL Molecular Graphics System, Schrödinger LLC Wwwpymolorg. Version 1. (2002) http://www.pymol.org. doi:citeulike-article-id:240061.

[23] J.C. Phillips, R. Braun, W. Wang, J. Gumbart, E. Tajkhorshid, E. Villa, et al., Scalable molecular dynamics with NAMD., J. Comput. Chem. 26 (2005) 1781–1802. doi:10.1002/jcc.20289.

[24] R.B. Best, X. Zhu, J. Shim, P.E.M. Lopes, J. Mittal, M. Feig, et al., Optimization of the additive CHARMM all-atom protein force field targeting improved sampling of the backbone phi, psi and side-chain chi(1) and chi(2) dihedral angles., J. Chem. Theory Comput. 8 (2012) 3257–3273. doi:10.1021/ct300400x.

[25] B. Kozlikova, E. Sebestova, V. Sustr, J. Brezovsky, O. Strnad, L. Daniel, et al., CAVER Analyst 1.0: graphic tool for interactive visualization and analysis of tunnels and channels in protein structures., Bioinformatics. 30 (2014) 2684–2685. doi:10.1093/bioinformatics/btu364.

[26] R.A. Laskowski, M.B. Swindells, LigPlot+: Multiple Ligand–Protein Interaction Diagrams for Drug Discovery, J. Chem. Inf. Model. 51 (2011) 2778–2786. doi:10.1021/ci200227u.

[27] J.M. Hayes, V.T. Skamnaki, G. Archontis, C. Lamprakis, J. Sarrou, N. Bischler, et al., Kinetics, in silico docking, molecular dynamics, and MM-GBSA binding studies on prototype indirubins, KT5720, and staurosporine as phosphorylase kinase ATP-binding site inhibitors: the role of water molecules examined., Proteins. 79 (2011) 703–719. doi:10.1002/prot.22890.

[28] G.M. Sastry, M. Adzhigirey, T. Day, R. Annabhimoju, W. Sherman, Protein and ligand

preparation: parameters, protocols, and influence on virtual screening enrichments., J. Comput. Aided. Mol. Des. 27 (2013) 221–234. doi:10.1007/s10822-013-9644-8.

[29] T.A. Halgren, R.B. Murphy, R.A. Friesner, H.S. Beard, L.L. Frye, W.T. Pollard, et al., Glide: a new approach for rapid, accurate docking and scoring. 2. Enrichment factors in database screening., J. Med. Chem. 47 (2004) 1750–1759. doi:10.1021/jm030644s.

[30] R. Appadurai, S. Senapati, Dynamical Network of HIV-1 Protease Mutants Reveals the Mechanism of Drug Resistance and Unhindered Activity., Biochemistry. 55 (2016) 1529–1540. doi:10.1021/acs.biochem.5b00946.

[31] I.T. Weber, D.W. Kneller, A. Wong-Sam, Highly resistant HIV-1 proteases and strategies for their inhibition, Future Med. Chem. 7 (2015) 1023–1038. doi:10.4155/fmc.15.44.

[32] M. Prabu-Jeyabalan, E. Nalivaika, C.A. Schiffer, Substrate Shape Determines Specificity of Recognition for HIV-1 Protease, Structure. 10 (2002) 369–381. doi:10.1016/S0969-2126(02)00720-7.

[33] M. Prabu-Jeyabalan, E. Nalivaika, C.A. Schiffer, Substrate shape determines specificity of recognition for HIV-1 protease: analysis of crystal structures of six substrate complexes., Structure. 10 (2002) 369–381.

ABSTRACT

A FIVE RESIDUE INSERTION BETWEEN CODONS 28 AND 29 OF THE HIV-1 PROTEASE GENE REDUCES THE REPLICATIVE CAPACITY OF THE VIRUS

by

CATHY MCLEOD

August 2016

Advisor: Dr. Ladislau Kovari

Major: Biochemistry and Molecular Biology

Degree: Master of Science

HIV-1 protease (PR) is a 99 amino acid protein responsible for cleavage of the viral polyprotein. We have identified a novel clinical isolate, MDR/28, which contains a five residue insertion between codons 28 and 29 of a multi-drug resistant (MDR) PR. This clinical isolate displays reduced viral replicative capacity compared to the wild-type. As opposed to drug-resistance mutations, studies on insertions remain largely underrepresented in the literature, and the consequences of such insertions are largely unknown. To understand the mechanism leading to reduced replicative capacity, three PR models were created and subjected to 40ns molecular dynamics simulations: MDR/28, wild type, and MDR PR. In addition, PR inhibitors (PI) atazanavir (ATV), darunavir (DRV), lopinavir (LPV) and saquinavir (SQV), as well as cleavage peptide CA/p2 were docked to the three models. The MDR/28-PI complexes displayed decreased binding affinity when compared to WT complexes, likely due to an increased active site cavity volume and altered secondary structure at residues local to the insertion mutant. Additionally, in the active site of MDR/28 the predicted binding mode of the CA/p2 peptide did not include contact with the catalytic residues, and migrated from that position, a behavior not

seen with any tested PIs or with either of the other PR models. These structural changes produced by the insertion suggest a mechanism for reduced replicative capacity of the mutant virus.

AUTOBIOGRAPHICAL STATEMENT

Cathy McLeod is a graduate student at the Wayne State University School of Medicine. She received a bachelor's degree in biology from the University of Detroit Mercy. Her research interests include viral drug targets, and structural biology. Her future directions include pursing continuing education and employment in the private sector.